Revisiting linearized one-dimensional tidal propagation

Marco Toffolon[1] and Hubert H. G. Savenije[2,3]

Received 23 August 2010; revised 15 March 2011; accepted 6 April 2011; published 12 July 2011.

[1] In this paper we extend the validity of the classical linear solution for tidal hydrodynamics including the effects of width and depth convergence. Reworking such a solution in the light of externally defined, dimensionless parameters we are able to provide simple relationships to predict the most relevant features of the tidal wave at the estuary mouth (velocity amplitude, phase lag, wavelength, and damping) and to reproduce the main dynamics of tidal wave propagation along finite and infinite length channels. We also highlight the need for an accurate treatment of the linearized bed shear stress by exploiting an iterative procedure, and we show the improvement that can be reached by subdividing the entire estuary in shorter reaches. Different versions of the analytical solution are compared with numerical results, highlighting the strengths and weaknesses of the linear model.

Citation: Toffolon, M., and H. H. G. Savenije (2011), Revisiting linearized one-dimensional tidal propagation, *J. Geophys. Res.*, *116*, C07007, doi:10.1029/2010JC006616.

1. Introduction

[2] Analytical solutions for tidal hydrodynamics have been the subject of extensive study exploiting different assumptions for different classes of estuaries [e.g., *Lanzoni and Seminara*, 1998]. The influence of along-channel geometrical variations (primarily funneling) has been the object of several papers, which studied in particular infinitely long estuaries for which elegant solutions can be found [e.g., *Jay*, 1991; *Friedrichs and Aubrey*, 1994; *Lanzoni and Seminara*, 1998; *Kukulka and Jay*, 2003; *Savenije et al.*, 2008]. In the case of a landward barrier or when riverine discharge has to be considered, the presence of a reflected wave tends to make the problem more complicated. A way to overcome this difficulty is to linearize the governing equations, an approach that has been applied even recently [e.g., *Souza and Hill*, 2006]. In fact, classical linear solutions [*Dronkers*, 1964], based on the assumption that the tidal amplitude is small with respect to the flow depth, have been the reference test for a long time, until the appearance of personal computers. From that time onward, numerical simulations gained ground because of their capability to describe complex dynamics, but the interest for simplified, explicit solutions for estuarine hydrodynamics remained.

[3] One of the main issues in deriving a linearized solution is the treatment of the friction term. In his seminal work, *Lorentz* [1926] proposed a linearization of the bed shear stress which has been the basis for simple solutions for many decades. This approach requires a suitable estimate of the linearization constant through a reference velocity, which is unknown. Although iterative approaches for its determination have been proposed, this is often assumed as a calibration parameter. A problem of a different nature comes from the need to follow along-channel variations of the estuarine sections, and has been tackled by subdividing the estuary in multiple reaches. These solution techniques (iteratively determined friction and multisection models) have been used by many researchers [e.g., *Giese and Jay*, 1989; *Jay and Flimchem*, 1997].

[4] In this paper we propose a modified derivation of the linear model, taking into account the effect of the variation of channel width and depth explicitly. Working in the context of a harmonic analysis, we investigate the behavior of the first harmonic (usually the most important component for water level and velocity oscillations) of the tidal signal, assumed to be the sum of sine waves characterized by stationary parameters. In order to derive simple yet general relationships, we analyze the problem using a dimensionless formulation that separates external and internal parameters [*Toffolon et al.*, 2006]. We examine three different models, which differ from each other because of the iterative refinement of the friction term and the subdivision of the estuary in multiple reaches. Therefore, given the tidal forcing and the geometry of the channel, we provide simple relationships for velocity amplitude, phase lag, wavelength, and damping, whose knowledge is especially important at the estuary mouth. We compare such results with a recent analytical solution [*Savenije et al.*, 2008] and with the solution of a fully nonlinear numerical model.

2. Formulation of the Problem

[5] We describe the tidal wave propagation by means of the usual one-dimensional continuity and momentum equations

$$\sigma \frac{\partial D}{\partial t} + U \frac{\partial D}{\partial x} + D \frac{\partial U}{\partial x} + \frac{UD}{B} \frac{\mathrm{d}B}{\mathrm{d}x} = 0, \tag{1}$$

$$\frac{\partial U}{\partial t} + U \frac{\partial U}{\partial x} + g \frac{\partial H}{\partial x} + \frac{\tau}{\rho D} = 0, \tag{2}$$

[1]Department of Civil and Environmental Engineering, University of Trento, Trento, Italy.
[2]Department of Water Management, Delft University of Technology, Delft, Netherlands.
[3]IHE Institute for Water Education, UNESCO, Delft, Netherlands.

0148-0227/11/2010JC006616

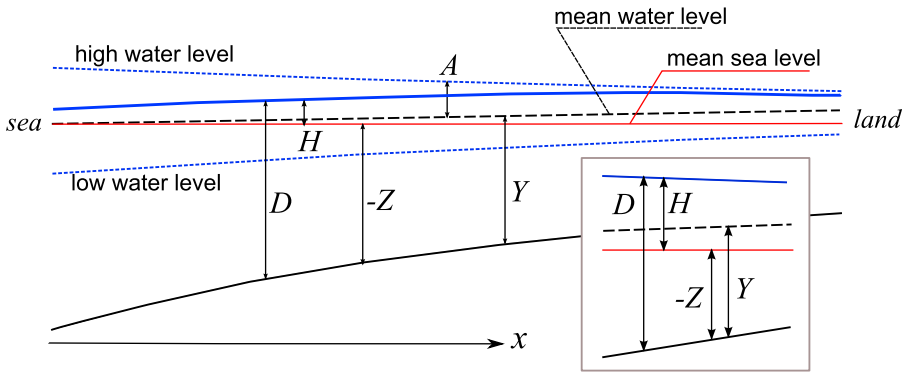

Figure 1. Sketch of water levels in the tidal channel.

where D is the depth, U the velocity, H the free surface elevation, ρ the water density, g the gravity acceleration, t is time, x is the longitudinal coordinate directed landward, and

$$\frac{\tau}{\rho} = \frac{|U|U}{C_h^2} \tag{3}$$

is the bed shear stress (C_h is the dimensionless Chézy parameter). We assume that the flow is concentrated in a main rectangular cross section with area BD, with a possible presence of lateral storage areas [*Speer and Aubrey*, 1985], whose effect is described by the storage ratio σ [e.g., *Savenije et al.*, 2008], and mainly determines an increase of flow velocity [*Seminara et al.*, 2010]. The possible dynamic effect of the storage areas on the momentum equation (2) is neglected as a first approximation [see also *Toffolon and Lanzoni*, 2010].

[6] We also assume that the hydrodynamics is tide dominated and that the semidiurnal M_2 tidal component is dominant, with frequency $\omega = 2\pi/T$ and period $T \simeq 12.4$ h. Then, introducing the mean depth $Y = \langle D \rangle$ (where angle brackets represent tidal average), the water level oscillations are described by the tidal amplitude A with respect to the mean depth Y, and the bed elevation (fixed in time, but varying along the channel) is given by $(-Z) = H - D = \langle H \rangle - Y$ (see Figure 1). The amplitude of the semidiurnal component of velocity oscillations is represented by the variable V.

[7] In order to recast the problem in dimensionless form, we use the values of average depth D_s (= Y_s), width B_s, and wave amplitude A_s at the seaward end of the channel as reference scales (identified by a subscript s). The resulting scale for the (a priori unknown) velocity amplitude V_s is given by $\sigma\epsilon C_s$ [*Savenije et al.*, 2008], where C_s is the frictionless wave celerity

$$C_s = \sqrt{\frac{gD_s}{\sigma}} \tag{4}$$

and ϵ is the dimensionless tidal amplitude (see also Table 1). The natural choice for the length scale is $L_s = C_s/\omega$. As usual, we describe the width of funnel-shaped estuaries by means of an exponential convergence law $B = B_s \exp(-x/L_b)$. In this case $B^{-1}\,\mathrm{d}B/\mathrm{d}x = L_b^{-1}$ is a constant, and the convergence term in (1) is null for $L_b \to \infty$. In the case of an estuary of finite length, then its length is indicated by L_e.

[8] In the case of negligible river discharge, the estuarine hydrodynamics are controlled by a few dimensionless parameters [*Toffolon et al.*, 2006; *Savenije et al.*, 2008]. The parameters that depend only on the geometry and on the external forcing are listed in Table 1, with reference to the scales defined at the seaward end of the channel. Other parameters, which depend on the resulting tidal motion in the channel (mainly because they are concerned with the velocity), are listed in Table 2, where ϕ_A and ϕ_V are the phases of the water level and velocity oscillations, respectively, and L_A and L_V are the actual wavelength of water level and velocity, respectively. It is also worth noting that λ can be seen as the ratio between the frictionless wave

Table 1. Independent Dimensionless Parameters

Parameter	Expression
tidal amplitude	$\epsilon = \dfrac{A_s}{D_s}$
friction	$\chi = \dfrac{\sigma\epsilon C_s}{C_h^2 \omega D_s}$
cross section convergence	$\gamma = \gamma_B + \gamma_Z$
lateral convergence	$\gamma_B = -\dfrac{L_s}{B_s}\dfrac{\mathrm{d}B}{\mathrm{d}x}\Big\|_s = \dfrac{L_s}{L_b}$
vertical convergence	$\gamma_Z = -\dfrac{L_s}{Z}\dfrac{\mathrm{d}Z}{\mathrm{d}x}\Big\|_s$

Table 2. Dependent Dimensionless Parameters

Parameter	Expression
velocity	$\mu = \dfrac{V_s}{\sigma\epsilon C_s}$
damping	$\delta = \dfrac{\delta_A + \delta_V}{2}$
damping water level	$\delta_A = \dfrac{L_s}{A_s}\dfrac{\mathrm{d}A}{\mathrm{d}x}\Big\|_s$
damping velocity	$\delta_V = \dfrac{L_s}{V_s}\dfrac{\mathrm{d}V}{\mathrm{d}x}\Big\|_s$
wavenumber	$\lambda = \dfrac{\lambda_A + \lambda_V}{2}$
wavenumber water level	$\lambda_A = 2\pi\dfrac{L_s}{L_A}$
wavenumber velocity	$\lambda_V = 2\pi\dfrac{L_s}{L_V}$
phase lag	$\phi = \phi_V - \phi_A$

celerity C_s and the actual wave speed [*Savenije et al.*, 2008], i.e., $\lambda_A = C_s/C_A$, $\lambda_V = C_s/C_V$, C_A and C_V being the celerities of the water level and velocity waves, respectively.

[9] In order to find a simple analytical solution, we adopt the usual Lorentz's linearization of the bed shear stress [*Lorentz*, 1926]

$$\frac{\tau}{\rho} = rU, \quad r = \kappa\frac{\widehat{U}}{C_h^2}, \quad \kappa = \frac{8}{3\pi}, \tag{5}$$

where $\widehat{U}$ is a reference maximum velocity, which should strictly vary with x, but it is usually assumed as a constant. A natural choice is to select $\widehat{U} = V_s$, which is however unknown a priori. Then, a dimensionless friction parameter can be defined for the linear stress as follows:

$$\widehat{\chi} = \frac{r}{\omega D_s} = \kappa\frac{V_s}{C_h^2\omega D_s}. \tag{6}$$

It is clear that $\widehat{\chi}$ is not an external parameter, since it depends on the resulting velocity V_s. Nevertheless, a simple relationship exists with χ in the form

$$\widehat{\chi} = \kappa\mu\chi. \tag{7}$$

2.1. Linear Solution

[10] In order to linearize the differential system, we assume that the tidal oscillations are small with respect to the depth ($\epsilon \ll 1$) and introduce the following structure for the unknowns (a superscript star denotes dimensionless variables):

$$\begin{aligned} H &= \epsilon D_s[A^* \exp(\mathrm{i}\omega t) + \mathrm{cc}]/2 + \mathrm{hot},\\ D &= D_s Y^* + \epsilon D_s[A^* \exp(\mathrm{i}\omega t) + \mathrm{cc}]/2 + \mathrm{hot},\\ U &= \sigma\epsilon C_s[V^* \exp(\mathrm{i}\omega t) + \mathrm{cc}]/2 + \mathrm{hot}, \end{aligned} \tag{8}$$

where A^* and V^* are unknown complex functions (cc represents the complex conjugate of the preceding term), and hot represent higher-order terms (residual head and velocity, overtides), not considered in the present analysis because their order of magnitude is assumed to be much smaller than the tidal amplitudes (A^*, V^*). Thus the average dimensionless depth is simply $\langle Y^*\rangle = Z^*$. The function A^*, Y^* and V^* vary along the dimensionless coordinate $x^* = x/L_s$. The structure of (8) implies that the hydrodynamics are dominated by a single sinusoidal tidal constituent (M_2), and the actual dimensional oscillations of water level and velocity are given by

$$A\cos(\omega t + \phi_A) = \epsilon D_s[A^* \exp(\mathrm{i}\omega t) + \mathrm{cc}]/2, \tag{9}$$

$$V\cos(\omega t + \phi_V) = \sigma\epsilon C_s[V^* \exp(\mathrm{i}\omega t) + \mathrm{cc}]/2, \tag{10}$$

where also ϕ_A and ϕ_V are functions of x^*.

[11] The differential system (1)–(2) can be easily linearized. The equations governing the variation of the tidal amplitudes (which are complex functions) are obtained by selecting the terms proportional to $\exp(\mathrm{i}\omega t)$

$$\mathrm{i}A^* + Z^*\frac{\partial V^*}{\partial x^*} - \gamma V^* Z^* = 0, \tag{11}$$

$$\mathrm{i}V^* + \frac{\partial A^*}{\partial x^*} + \widehat{\chi}\frac{V^*}{Z^*} = 0, \tag{12}$$

where γ and $\widehat{\chi}$ may vary with x^* in principle.

[12] The two equations (11) and (12) can be combined into a single, second-order differential equation and solved for one of the two unknowns if the coefficients are constant. This means that we have to neglect any variation of the parameters $\widehat{\chi}$ and γ, and of the average depth Z^* (except that implicitly included in γ_Z) along x^*. This is a key point of the analysis, since the above assumptions are in general not strictly valid. Nevertheless, we will proceed with an approximate solution, which is indeed correct for short estuary reaches, whereby we can assume $Z^* = 1$ and assign the well-known structure of the constant-coefficient solution to both variables as follows:

$$A^* = a_1^* \exp(w_1^* x^*) + a_2^* \exp(w_2^* x^*), \tag{13}$$

$$V^* = v_1^* \exp(w_1^* x^*) + v_2^* \exp(w_2^* x^*), \tag{14}$$

where $w_l^* = m_l^* + \mathrm{i}k_l^*$ ($l = 1,2$) is a complex number, with m_l^* representing the amplification factor and k_l^* the wavenumber. In this case the continuity equation gives the relationship

$$a_l^* = \mathrm{i}(w_l^* - \gamma)Z^* v_l^*, \tag{15}$$

which is valid locally and hence we retain the variable depth Z^* (it will be used when applying the landward boundary condition). Substituting the information from (15) into the momentum equation, the second-order equation

$$w_l^{*2} - \gamma w_l^* + 1 - \mathrm{i}\widehat{\chi} = 0 \tag{16}$$

can be obtained, which gives the solution

$$w_l^* = \frac{\gamma}{2} \pm \Delta, \quad \Delta = \sqrt{-\Gamma + \mathrm{i}\widehat{\chi}}, \tag{17}$$

where the parameter

$$\Gamma = 1 - \left(\frac{\gamma}{2}\right)^2 \tag{18}$$

measures the distance from frictionless critical convergence $\gamma = 2$ [*Jay*, 1991; *Savenije et al.*, 2008].

[13] In more detail, (17) gives two solutions: the first with the positive root and the second with the negative root

$$w_1^* = \frac{\gamma}{2} + \Delta, \quad w_2^* = \frac{\gamma}{2} - \Delta. \tag{19}$$

Consequently, equation (15) gives the following relationships:

$$v_1^* = \frac{\mathrm{i}a_1^*}{(\gamma/2 - \Delta)Z^*}, \quad v_2^* = \frac{\mathrm{i}a_2^*}{(\gamma/2 + \Delta)Z^*}. \tag{20}$$

The parameter Δ can be separated into its real and imaginary parts

$$\Re(\Delta) = K, \quad \Im(\Delta) = \frac{\widehat{\chi}}{2\Re(\Delta)} = \sqrt{\frac{\Omega + \Gamma}{2}}, \tag{21}$$

where

$$\Omega = \sqrt{\Gamma^2 + \widehat{\chi}^2}, \quad K = \sqrt{\frac{\Omega - \Gamma}{2}}. \tag{22}$$

The relationships (21) imply that $m_l^* = \gamma/2 \pm \Re(\Delta)$ and $k_l^* = \pm \Im(\Delta)$ (with plus sign for $l = 1$ and minus for $l = 2$). We note that $\Gamma^2 + \widehat{\chi}^2 \geq 0$ always, so Ω is a real number, and that $\Omega \geq |\Gamma|$ always, so the right hand sides of (21) are indeed real functions.

2.2. Boundary Conditions

[14] The amplitudes a_l^* and v_l^* are determined exactly by means of two boundary conditions applied at the reach ends. We can impose the boundary condition in terms of a known free surface elevation in a generic section x_h as follows:

$$H = \epsilon D_s h^* [\exp \mathrm{i}(\omega t + \theta_h) + \mathrm{cc}]/2 \quad (x^* = x_h^*), \tag{23}$$

where h^* is the dimensionless amplitude of the tide, and θ_h is the phase. The relationship between a_1^* and a_2^* is then readily determined as

$$a_1^* \exp(\Delta x_h^*) + a_2^* \exp(-\Delta x_h^*) = h^* \exp\left(\mathrm{i}\theta_h - \frac{\gamma}{2} x_h^*\right). \tag{24}$$

The other relevant case is where a flux is imposed as a boundary condition in the form

$$UD = \sigma \epsilon C_s D_s Z^* q^* \left[\exp \mathrm{i}\left(\omega t + \theta_q\right) + \mathrm{cc}\right]/2 \quad \left(x^* = x_q^*\right), \tag{25}$$

where q^* is the amplitude of the imposed dimensionless flux and θ_q its phase. After linearization $UD = \sigma \epsilon C_s D_s Z^* [V^* \exp(\mathrm{i}\omega t) + \mathrm{cc}]/2$, and hence

$$v_1^* \exp\left(\Delta x_q^*\right) + v_2^* \exp\left(-\Delta x_q^*\right) = \frac{q^*}{Z^*|_{x_q^*}} \exp\left(\mathrm{i}\theta_q - \frac{\gamma}{2} x_q^*\right) \tag{26}$$

or exploiting (20), which allows one to cancel Z^*,

$$\frac{\exp\left(\Delta x_q^*\right)}{(\Delta - \gamma/2)} a_1^* - \frac{\exp\left(-\Delta x_q^*\right)}{(\Delta + \gamma/2)} a_2^* = \mathrm{i} q^* \exp\left(\mathrm{i}\theta_q - \frac{\gamma}{2}\right). \tag{27}$$

[15] The actual solution of the problem is determined by a physically reasonable combination of (24) and (27) for depth and velocity oscillations. Once the complex functions A^* and V^* have been determined by means of suitable boundary conditions, the physical waves are defined by (9)–(10), and the amplitudes and phases can be calculated as follows:

$$A = \epsilon D_s |A^*|, \quad V = \sigma \epsilon C_s |V^*|, \tag{28}$$

$$\tan(\phi_A) = \frac{\Im(A^*)}{\Re(A^*)}, \quad \tan(\phi_V) = \frac{\Im(V^*)}{\Re(V^*)}. \tag{29}$$

[16] The dimensionless parameters defined in Table 2 are calculated using the functions A and V at the seaward end of the estuary reach. Then, the dimensionless scale of velocity is $\mu = |V^*|$, the phase lag is $\phi = \phi_V - \phi_A$, the damping coefficients and the wavenumbers of the two waves can be calculated as

$$\delta_A = \Re\left(\frac{1}{A^*} \frac{dA^*}{dx^*}\right), \quad \delta_V = \Re\left(\frac{1}{V^*} \frac{dV^*}{dx^*}\right), \tag{30}$$

$$\lambda_A = \Im\left(\frac{1}{A^*} \frac{dA^*}{dx^*}\right), \quad \lambda_V = \Im\left(\frac{1}{V^*} \frac{dV^*}{dx^*}\right), \tag{31}$$

respectively. The derivation of (30)–(31) is given in Appendix A.

3. Results

[17] The solution obtained in section 2 represents a linear approximation of the fully nonlinear hydrodynamics. However, it is not expressed in terms of external parameters because $\widehat{\chi}$ contains the dimensionless scale of velocity μ at the seaward end of the channel, as described by (7).

[18] In general, an explicit solution for μ cannot be derived, thus an iterative refinement is needed to obtain the correct wave behavior. The following procedure usually converges in a few steps: (1) assume $\widehat{\chi} = \chi$ as a first attempt, and calculate $\mu = |V^*|$ using the analytical solution; (2) modify $\widehat{\chi}$ according to (7) and calculate a new tentative value for μ; and (3) when the process converges, calculate the other parameters δ, λ, and ϕ. Such an iterative refinement allows for the reintroduction of one of the aspects of the quadratic nonlinearity of the friction term in the solution, which therefore should not be considered strictly linear, although it is obviously not able to reproduce nonlinear effects such as the generation of overtides. The procedure is simple and does not require specific numerical codes (two examples of Matlab scripts are provided as auxiliary material): since the convergence is usually fast, a spreadsheet can be a suitable tool for the majority of practical problems.[1] Moreover, the problem with the constant-coefficient assumption (in particular $Z^* = 1$) can be overcome by subdividing the estuary in short reaches and then solving the overall problem.

[19] In sections 3.1, 3.2, 3.4, and 3.5 we compare the analytical solution with fully nonlinear numerical results using the numerical model described by *Toffolon et al.* [2006]. The numerical results are interpreted as follows: (1) a Fourier analysis is performed on water levels and velocities along the estuaries; (2) the amplitude and phase of the first tidal constituent (M_2) are calculated; and (3) the dimensionless parameters μ, δ, λ, ϕ are estimated following the definitions of Table 2. The residual water level and velocity and the overtides are not considered in the analysis. Moreover, for sake of simplicity we set $\sigma = 1$ (no storage areas).

[20] In section 3.1 we show how an accurate solution can be found with the linear model. Then, we will discuss the problem of characterizing the estuarine hydrodynamics with simple relationships and we will derive the dimensionless parameters at the mouth of the channel in some particular cases.

3.1. Sequence of Reaches

[21] In this section we set up the general problem of an estuary subdivided into N reaches. In this way the longitudinal variability can be fully taken into account, both for the variation of the external parameters (i.e., geometry) and for internal parameters (e.g., μ, assumed constant within each part). This also justifies the use of a constant Z^* in the derivation of the analytical solution. Therefore, the whole estuary is subdivided into a sequence of linear problems determined by suitable boundary conditions: external (sea-

[1] Auxiliary materials are available in the HTML. doi:10.1029/2010JC006616.

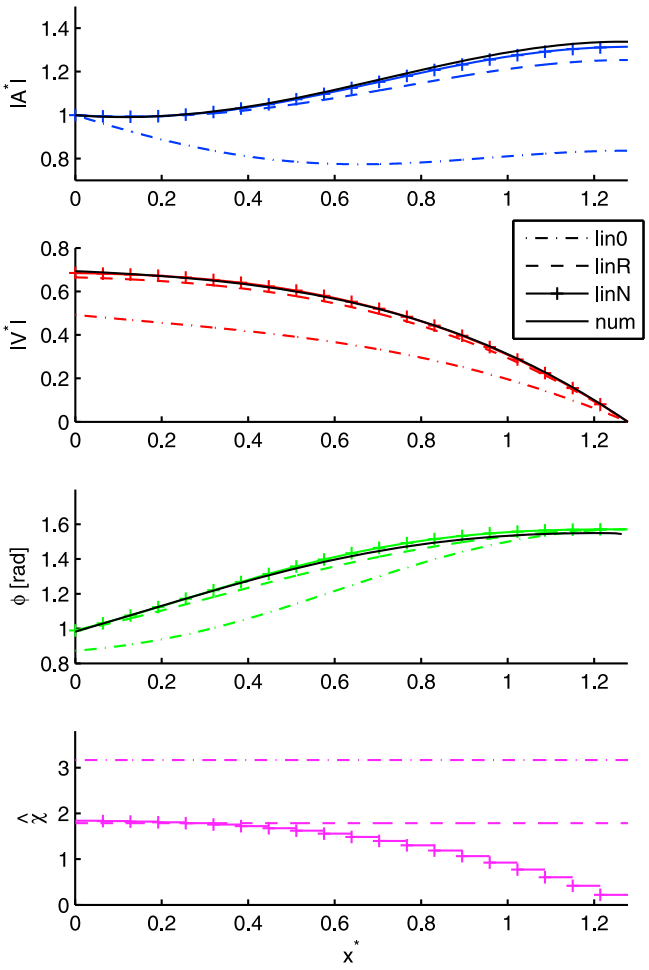

Figure 2. Dimensionless amplitudes $|A^*|$, $|V^*|$; phase lag ϕ; and linearized friction parameter $\widehat{\chi}$ along x^*: comparison among three versions of the linear model ("lin0," nonrefined; "linR," refined with single reach; "linN," refined with multiple reaches) and the numerical results ("num") for a channel with horizontal bed ($\gamma_Z = 0$). See also section 3.1.

ward and landward) and internal (at the nodes between reaches). We enumerate the reaches starting from the sea ($j = 1$) to the landward end ($j = N$). In order to find simpler relationships, we use a moving origin of the axis x^* for every reach, whose length is L_j^*. For simplicity, we assume the same value of ϵ (calculated at the estuary mouth) for all reaches. This means that the scale of water level variations is $\epsilon D_{s,j}$, with $D_{s,j}$ the actual depth of the seaward end of reach j, and hence $h^* \neq 1$ in the boundary condition (24) for the generic reach.

[22] Let us first consider the internal boundary conditions between a reach j and its upstream neighbor $j + 1$. Assuming that the water level cannot be discontinuous implies that

$$a_{1,j}^* \exp\left(w_{1,j}^* L_j^*\right) + a_{2,j}^* \exp\left(w_{2,j}^* L_j^*\right) = \\ = \alpha_j \left(a_{1,j+1}^* + a_{2,j+1}^*\right), \tag{32}$$

where $\alpha_j = D_{s,j+1}/D_{s,j}$ is the ratio assuring the dimensional correspondence. The same considerations hold for the discharge: assuming that both depth and width are continuous at the node yields the condition

$$\frac{\exp\left(w_{1,j}^* L_j^*\right)}{w_{2,j}^*} a_{1,j}^* + \frac{\exp\left(w_{2,j}^* L_j^*\right)}{w_{1,j}^*} a_{2,j}^* = \\ = \alpha_j^{1/2} \left[\frac{a_{1,j+1}^*}{w_{2,j+1}^*} + \frac{a_{2,j+1}^*}{w_{1,j+1}^*}\right] \tag{33}$$

for the velocity, where the exponent of α_j is 1/2 because the scale of velocity $\epsilon C_s \propto \sqrt{D_s}$. The set of equations (32)–(33) is defined for the internal nodes $j \in [1, N-1]$ and provides $2(N-1)$ relationships for the $2N$ unknowns. The two missing equations are given by the external boundary conditions: the forcing tide (24)

$$a_{1,1}^* + a_{2,1}^* = 1 \tag{34}$$

and the landward condition (27), which can be easily imposed either for a closed channel,

$$\frac{\exp\left(w_{1,N}^* L_N^*\right)}{w_{2,N}^*} a_{1,N}^* + \frac{\exp\left(w_{2,N}^* L_N^*\right)}{w_{1,N}^*} a_{2,N}^* = 0 \tag{35}$$

or for an ideally infinite reach, $a_{1,N}^* = 0$ (see also section 3.2). The linear system can be solved for the unknowns $a_{1,j}$, $a_{2,j}$ by means of a suitable numerical scheme. We note that a standard Gaussian elimination method can be used to solve the linear system [*Giese and Jay*, 1989]. In Appendix B we show an explicit recursive derivation, which however may give unreliable numerical results.

[23] It is worth looking at the performances of the different analytical solutions against fully nonlinear numerical results. In Figures 2 and 3 we compare the dimensionless amplitudes of water level and velocity oscillations and the phase lag in four cases: (1) nonrefined linear model ("lin0," assuming $\widetilde{\chi} = \chi$, i.e., $\mu = 1/\kappa$); (2) iteratively refined linear model with a single reach ("linR"); (3) iteratively refined linear model with multiple reaches ("linN," with $N = 20$); and (4) numerical simulations ("num"). The example is chosen to test the linear model in a complex case: $\epsilon = 0.2$ is not small ($A_s = 2$ m, $D_s = 10$ m); the channel is closed landward, so the reflected wave is important, but it is long enough ($L_e = 90$ km) to exhibit a non trivial behavior; friction is relevant ($\chi = 3.17$), and width convergence ($\gamma_B = 1.17$, given by $L_b = 60$ km) plays a role. The only difference between the Figures 2 and 3 is the inclusion of depth convergence in Figure 3 ($\gamma_Z = 0.78$ from an exponential variation of the bed level characterized by $L_z = 90$ km), compared with the horizontal bed of Figure 2. Assuming the numerical results as a benchmark, the comparison shows that in both cases the linN model performs almost perfectly, while the lin0 model is not satisfactory. A specific remark concerns the single-reach refined model (linR): with horizontal bed ($\gamma_Z = 0$, Figure 2) it works quite well, whereas when the depth convergence is significant (Figure 3) it strongly deviates from the correct solution while moving landward. It is worth noting however that this model reproduces the velocity amplitude at the mouth very satisfactorily in both cases: this fact, which implies that the total convergence γ has a strong significance in determining the wave behavior at the mouth, will be exploited in the following analysis.

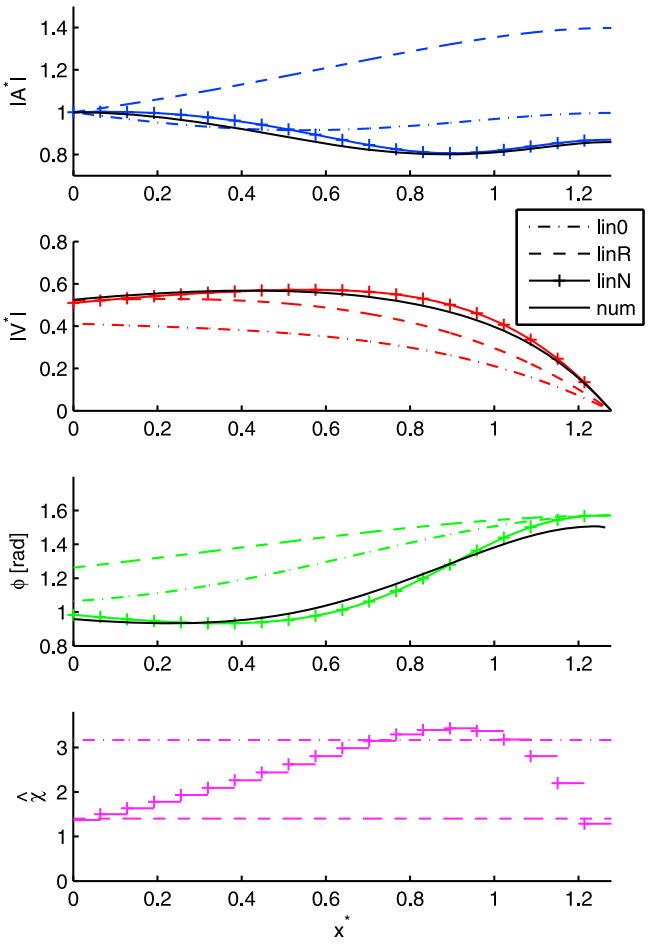

Figure 3. Dimensionless amplitudes $|A^*|$, $|V^*|$; phase lag ϕ; and linearized friction parameter $\widehat{\chi}$ along x^*: comparison for a channel with decreasing depth ($\gamma_Z > 0$). See also Figure 2 and section 3.1.

[24] Finally, the fourth subplot of Figures 2 and 3 shows how the linearized friction parameter $\widehat{\chi}$ changes along the channel for the linN model in comparison with the constant values assumed by the linR (where $\widehat{\chi}$ is iteratively refined at the mouth only) and lin0 ($\widehat{\chi} = \chi$). The variation is particularly interesting for the case with decreasing depth (Figure 3) since a maximum for $\widehat{\chi}$ exists due to the opposing effects of depth reduction (increasing χ) and velocity decay (decreasing μ).

3.2. Infinitely Long Channel

[25] Now we examine some particular cases. A relevant one is that of long channels, where there is not a landward boundary condition. This simple yet general case can be obtained by setting $h^* = 1$ (tidal amplitude at the mouth equal to the forcing amplitude scale) and $\theta_h = 0$ (which can be always obtained by shifting the origin of time), and choosing $x_h^* = 0$. Since the landward boundary condition is ideally imposed at ∞, and using (20), the solution is determined by

$$a_1^* = 0, \quad a_2^* = 1, \quad v_1^* = 0, \quad v_2^* = \frac{\mathrm{i}}{(\Delta + \gamma/2)}, \tag{36}$$

which suggest that there is no reflected wave ($a_1^* = v_1^* = 0$), and give

$$A^* = \exp(m_2^* x^* - \mathrm{i} k_2^* x^*), \tag{37}$$

$$V^* = \left(\frac{k_2^* + \mathrm{i} m_2^*}{m^{*2}_2 + k^{*2}_2} \right) \exp(m_2^* x^* - \mathrm{i} k_2^* x^*), \tag{38}$$

where $m_2^* = \Re(\Delta) + \gamma/2$ and $k_2{}^* = \Im(\Delta)$.

[26] Focusing attention on the dependent dimensionless parameters at the mouth, where the single-reach solution (linR) is reasonably accurate, it is straightforward to derive

$$\mu = \frac{1}{\sqrt{m^{*2}_2 + k^{*2}_2}} = \left(\Omega + \frac{\gamma^2}{4} + \gamma \sqrt{\frac{\Omega - \Gamma}{2}} \right)^{-1/2}. \tag{39}$$

The phase lag is given by $\phi = \phi_V - \phi_A$, where $\phi_A = 0$, and hence

$$\tan(\phi) = \frac{m_2^*}{k_2^*} = \frac{\Omega - \Gamma}{\widehat{\chi}} + \frac{\gamma}{\widehat{\chi}} \sqrt{\frac{\Omega - \Gamma}{2}}. \tag{40}$$

The damping $\delta = m_2^* = \gamma/2 - K$ and the wavenumber $\lambda^2 = k_2{}^{*2} = (\Omega + \Gamma)/2$ are the same for both water level and velocity. The complete set of the dependent dimensionless parameters for the general case is reported in Table 3.

[27] Now we can test the performance of some analytical solutions (the different versions of the present linear model, and the *Savenije et al.* [2008] model, which will be examined also later) against numerical results. In particular, we focus on the dimensionless parameters μ, δ, λ, and ϕ, evaluated at the mouth of the estuary. As for the numerical

Table 3. Dimensionless Parameters at the Mouth of an Infinitely Long Channel: The General Solution and Some Particular Cases

	μ	δ	λ^2	$\tan(\phi)$	Notes
general case	$\frac{1}{\sqrt{1 + \gamma K + 2K^2}}$	$\frac{\gamma}{2} - K$	$K^2 + \Gamma$	$\frac{\gamma K + 2K^2}{\widehat{\chi}}$	$K = \sqrt{\frac{\Omega - \Gamma}{2}}$, $\Omega = \sqrt{\Gamma^2 + \widehat{\chi}^2}$
frictionless ($\chi = 0$), subcritical ($\Gamma > 0$)	1	$\frac{\gamma}{2}$	Γ	$\frac{\gamma}{2\sqrt{\Gamma}}$	$\Omega = 0$, $K = 0$
frictionless ($\chi = 0$), supercritical ($\Gamma < 0$)	$\frac{\gamma}{2} - \sqrt{-\gamma}$	$\frac{\gamma}{2} - \sqrt{-\gamma}$	0	∞	$\Omega = -\Gamma$
constant cross section ($\Gamma = 1$)	$\Omega^{-1/2}$	$-\sqrt{\frac{\Omega - 1}{2}}$	$\frac{\Omega + 1}{2}$	$\frac{\Omega - 1}{\widehat{\chi}}$	$\Omega = \sqrt{1 + \widehat{\chi}^2}$
ideal estuary (no damping, $\delta = 0$)	$\frac{1}{\sqrt{\gamma^2 + 1}}$	0	1	$\frac{3}{4}\gamma$	$K = \frac{\gamma}{2}$, $\widehat{\chi} = \gamma$

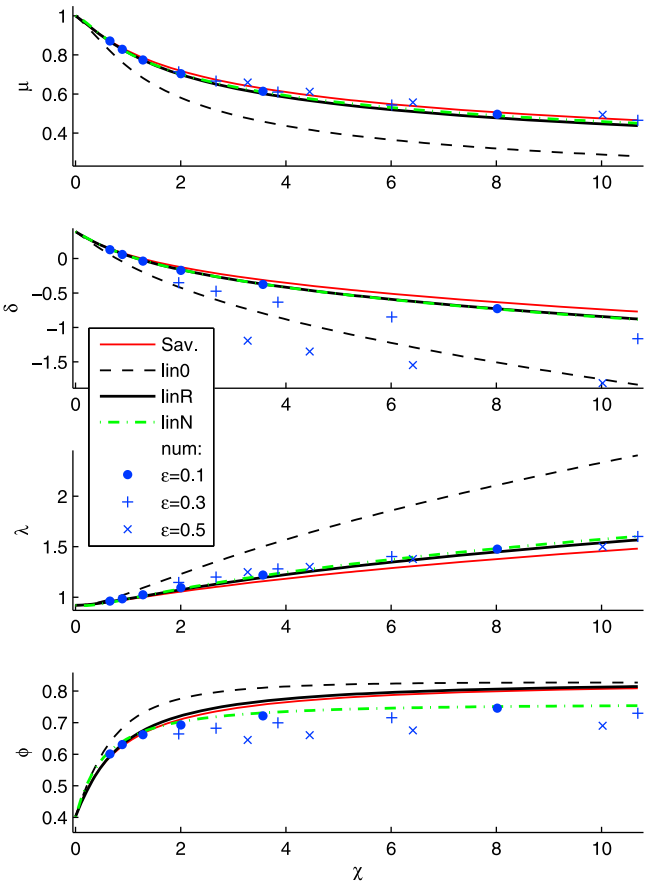

Figure 4. Infinitely long estuary: main dimensionless parameters (velocity μ, damping δ, wavenumber λ, phase lag ϕ) obtained with various analytical relationships as a function of friction parameter χ, for constant $\gamma = 0.78$ (with $\gamma_Z = 0$). "Sav.," the *Savenije et al.* [2008] solution; lin0, nonrefined linear model ($\widehat{\chi} = \chi$); linR, refined with single reach; linN, refined with multiple reaches ($L_N^* = 1$, $N = 20$); num, numerical with different values of ϵ.

model, we adopt a reference depth $D_s = 10$ m at the mouth, and let the other quantities vary (tidal amplitude, friction, width and depth convergence lengths); both the width and depth convergence are assumed exponential. The behavior of the dimensionless parameters is shown in Figure 4, 6, 7, where numerical results obtained with different values of ϵ (from 0.1 to 0.5) are denoted by different markers. An example of the increasing divergence of the linear solution from numerical results when ϵ becomes larger is given in Figure 5.

[28] The variation of the dependent dimensionless parameters with χ is shown in Figure 4 for a given value of γ (= 0.78). For this case the numerical values of the dimensionless scale of velocity μ are perfectly approximated by all analytical models except the usual lin0 (possible deviations of the *Savenije et al.* [2008] model around the critical convergence are discussed below), almost independently of ϵ. This is surprisingly true also for larger ϵ (Figure 5), at least until ϵ reaches excessive values (~0.8), which are far beyond the limits of a linear model assuming small values of this parameter. The same behavior occurs for the dimensionless wavenumber λ, with just a more sensible dependence on ϵ. The damping δ is well fit by the analytical solutions only for sufficiently small ϵ, but it clearly feels the increase of this parameter [see also *Toffolon et al.*, 2006]. The phase lag ϕ, apart from the dependence on ϵ, is well reproduced (in the limits of applicability of the linear model) only by the linN model, although the deviation of the linR model is not too large. This suggests that the solution at the mouth is affected by the behavior along the channel, and in particular by the damping of the velocity for stronger friction (see the plot of δ), which changes the effective x-dependent friction parameter $\widehat{\chi}$.

[29] Figures 6 and 7 describe the variation of the dependent dimensionless parameters with γ when χ (= 3.56) is fixed: the former consider the case of horizontal bed ($\gamma_Z = 0$, $\gamma = \gamma_B$), while the latter the other limit, i.e., constant width ($\gamma_B = 0$, $\gamma = \gamma_Z$). It is evident from Figure 6 that the linR and linN models work perfectly for μ, λ, and ϕ (where a small deviation of linR appears for small γ). The damping δ, well reproduced by both models for small ϵ, tends to deviate for larger tidal amplitudes. It is interesting to discuss the deviations of the *Savenije et al.* [2008] model around $\gamma = 2.3$ (the critical convergence for the assigned χ): the discontinuous behavior and the transition toward a standing wave do not seem to be physically reasonable (at least in the numerical approximation).

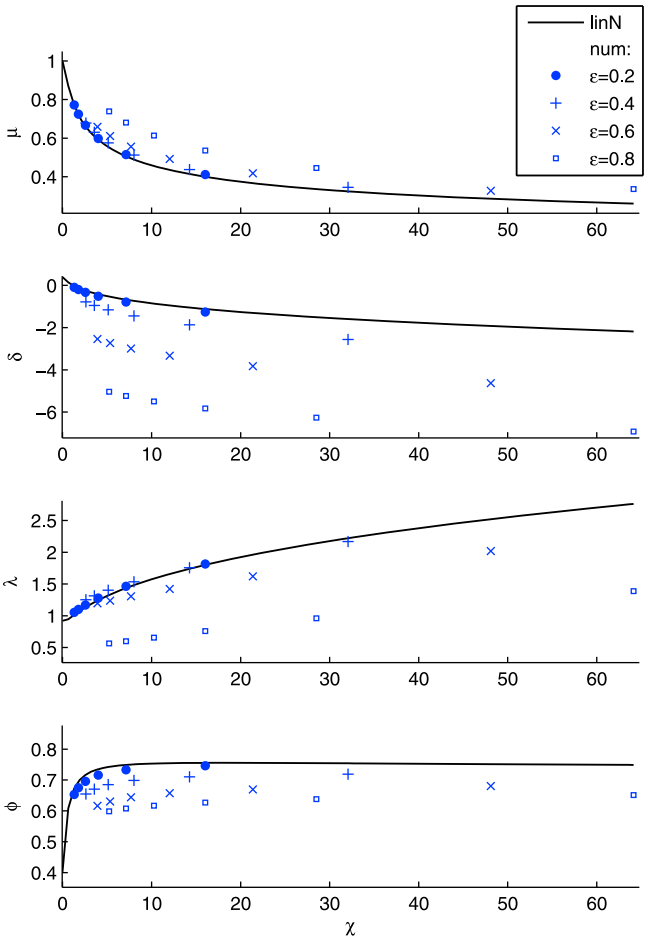

Figure 5. Infinitely long estuary: the linN model as in Figure 4 compared with numerical results with large values of ϵ.

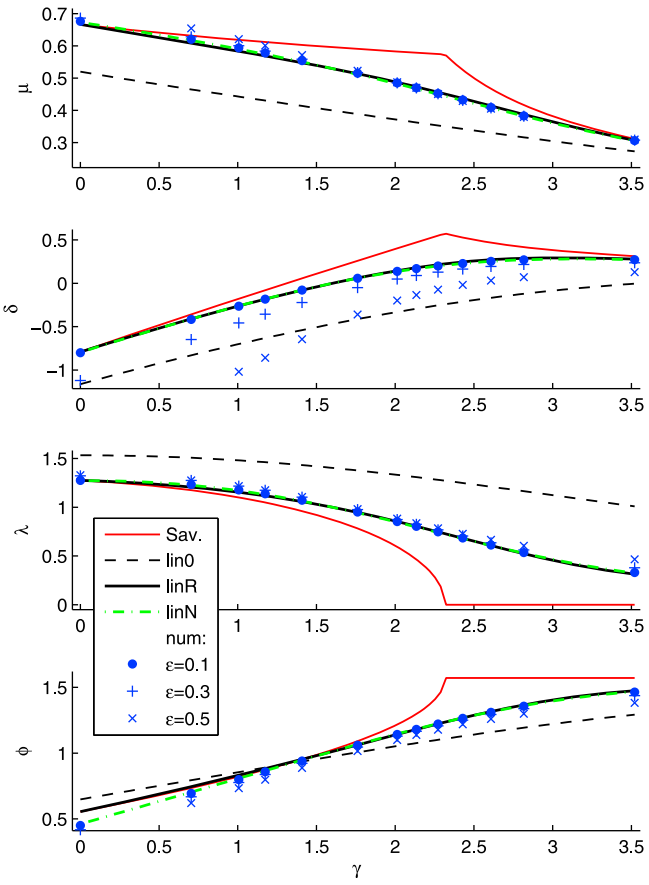

Figure 6. Infinitely long estuary: main dimensionless parameters (velocity μ, damping δ, wavenumber λ, phase lag ϕ) obtained with various analytical relationships as a function of convergence γ (with $\gamma_Z = 0$), for constant $\chi = 3.56$, compared with numerical results. For the legend see Figure 4.

[30] Figure 7 shows the limitation of assuming a constant Z^* to find the solution of the differential system (11)–(12). Now the comparison between numerical and analytical results is worse, especially for large γ_Z (very steep bed) and specific parameters (in particular the wavenumber λ). However, although the case of a strong exponential variation of the depth is mainly academic, the analytical model retains some of the effects of the variable bed level on hydrodynamics, which would have been totally disregarded adopting a constant-depth model.

3.3. Particular Cases for Infinite Channel

[31] It is worth examining some particular cases, for which analytical solutions have already been derived. In particular, we refer to the solution discussed by *Savenije et al.* [2008], where these cases have already been identified and compared with previous results. Incidentally, we note that the assumption $\delta_A = \delta_V$ introduced to derive the *Savenije et al.* [2008] solution is not an independent requirement, but just a consequence of having considered the case of infinite length estuaries.

[32] We identify the following specific conditions: (1) the frictionless case ($\chi = 0$), where we can distinguish the case of subcritical convergence ($\gamma < 2$, condition 1a) and the case of supercritical convergence ($\gamma > 2$, condition 1b); (2) the case of constant cross section ($\gamma = 0$); and (3) the case of ideal estuary (i.e., without damping, $\delta = 0$). All these particular solutions are reported in Table 3.

3.3.1. Condition 1a: Frictionless, Subcritical Convergence

[33] The solution can be easily obtained by setting $\widehat{\chi} = 0$ (hence $\Omega = \Gamma$ for $\Gamma > 0$, and $K = 0$). In the same case, *Savenije et al.* [2008] find exactly the same relationships as an asymptotic case of the mixed wave solution.

3.3.2. Condition 1b: Frictionless, Supercritical Convergence

[34] The solution is derived by setting $\Gamma < 0$ and $\chi = 0$, which yield $\Omega = -\Gamma = \gamma^2/4 - 1$ and $K = \sqrt{-\Gamma}$, and hence the wavelength tends to be infinite ($\lambda = 0$, see Table 3). Differently, the relationships proposed by *Savenije et al.* [2008] for the case of apparent standing wave are always characterized by $\lambda = 0$ when the threshold condition $\chi < -2\gamma\Gamma + (\gamma^2 - 2)\sqrt{-\Gamma}$ is satisfied, even with friction. Actually, in the present model a clear separation between the subcritical and the supercritical cases exists only for vanishing friction ($\chi = 0$). In fact, when $\Gamma < 0$ but friction is present

$$\lambda^2 = \frac{-\Gamma}{2}\left[-1 + \sqrt{1 + \frac{\widehat{\chi}^2}{\Gamma^2}}\right], \tag{41}$$

which can attain very small values (i.e., very long wavelength) as far as $\widehat{\chi}^2 \ll \Gamma^2$, but it is always $\lambda^2 > 0$. Therefore,

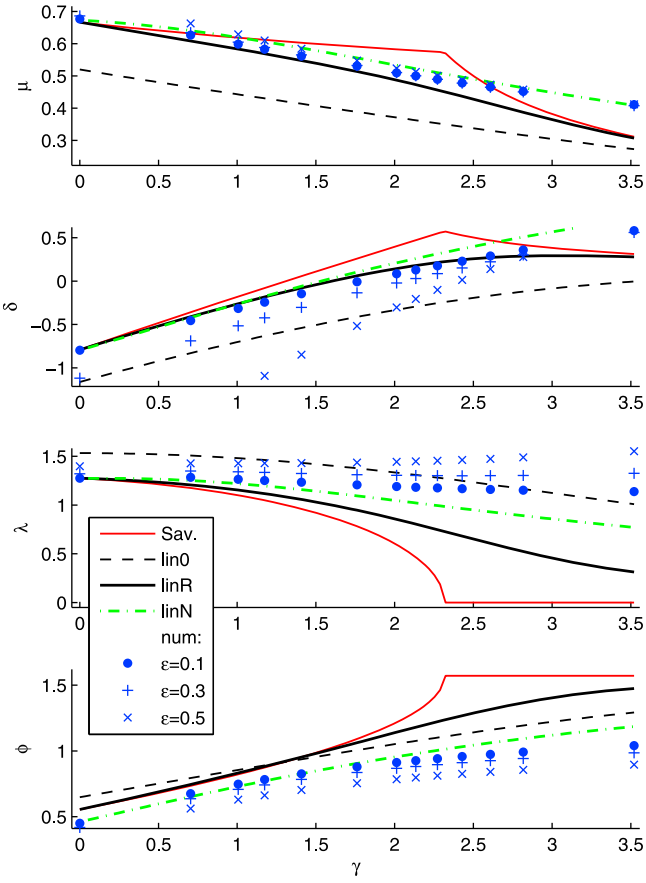

Figure 7. Infinitely long estuary: main dimensionless parameters as in Figure 6 but with $\gamma = \gamma_Z$ ($\gamma_B = 0$; $\chi = 3.56$).

Savenije et al. [2008] apparent standing wave is verified exactly only for the idealized case of complete lack of friction ($\chi = 0$, or in approximate form $\widehat{\chi}^2 \ll \Gamma^2$).

3.3.3. Condition 2: Constant Cross Section

[35] Since the present model considers the effect of width and depth variations together, we can set $\gamma = 0$ (hence $\Gamma = 1$, $\Omega = \sqrt{1+\widehat{\chi}^2}$) to find the solution for this case. The analogous case treated by *Savenije et al.* [2008] suggests a different set of relationships, which can be rewritten as

$$\mu_0 = \sqrt{\frac{-2\delta_0}{\chi}}, \quad \lambda_0^2 = 1+\delta_0^2, \quad \tan(\phi_0) = -\frac{\delta_0}{\sqrt{1+\delta_0^2}},$$
$$\delta_0 = \frac{\sqrt[3]{R_0-\chi} - \sqrt[3]{R_0+\chi}}{2}, \quad R_0 = \sqrt{\chi^2 + \frac{8}{27}}. \tag{42}$$

The two sets of solutions are different, but they tend to coincide for weak friction since (42) give

$$\mu = 1 - \frac{\chi^2}{4} + O(\chi^4), \quad \delta = -\frac{\chi}{2} + O(\chi^3),$$
$$\lambda = 1 + \frac{\chi^2}{8} + O(\chi^4), \quad \phi = \frac{\chi}{2} + O(\chi^3), \tag{43}$$

and the solution in Table 3 gives the same expansions in terms of $\widehat{\chi}$. When χ cannot be approximated by $\widehat{\chi}$, the solution reported in Table 3 should be refined recalling (7). Instead of using iteration, in this case the solution can be obtained in closed form by solving

$$\kappa^2\chi^2\mu^6 + \mu^4 - 1 = 0, \tag{44}$$

which is comparable with the relationship used by *Savenije et al.* [2008], $\chi^2\,\mu^6 + 2\mu^2 - 2 = 0$. The real root of (44) gives

$$\mu = \frac{1}{\chi_\kappa}\sqrt{\frac{1}{3}\left(\frac{m_1}{2} + \frac{2}{m_1} - 1\right)}, \quad \delta = -\frac{1}{\mu}\sqrt{\frac{1-\mu^2}{2}},$$
$$\lambda^2 = \frac{1+\mu^2}{2\mu^2}, \quad \tan(\phi) = \frac{1-\mu^2}{\chi_\kappa\mu^3}, \quad \chi_\kappa = \kappa\chi,$$
$$m_1 = 3\left[4\chi_\kappa^4 - \frac{8}{27} + 4\chi_\kappa^2\sqrt{\chi_\kappa^4 - \frac{4}{27}}\right]^{1/3}. \tag{45}$$

The comparison between the *Savenije et al.* [2008] relationships and the linearized ones for the case of constant cross section suggests that the iteratively refined solution (45) is very similar to *Savenije et al.*'s [2008] results. Finally, when $\chi \to 0$ (frictionless limit) the well-known result $\mu = \lambda = 1$, $\delta = \phi = 0$ is obtained.

3.3.4. Condition 3: Ideal Estuary

[36] The condition of no damping is easily set by posing $\delta = 0$, which implies $K = \gamma/2$ and $\widehat{\chi}^2 = \gamma^2$. Using (7), and noting that γ must be positive in order to balance the damping due to friction, the relationship becomes

$$\chi = \frac{\gamma}{\kappa}\sqrt{\gamma^2+1}. \tag{46}$$

The results of the linear model are given again in Table 3. The relationships found by *Savenije et al.* [2008] are

$$\mu_I = \frac{1}{\sqrt{\gamma^2+1}}, \quad \delta_I = 0, \quad \lambda_I^2 = 1, \quad \tan(\phi_I) = \gamma, \tag{47}$$

with

$$\chi_I = \gamma(\gamma^2+1), \tag{48}$$

which is different from (46). For small friction (small χ and hence small γ), (46) can be expanded as

$$\chi = \frac{\gamma}{\kappa} + \frac{\gamma^3}{2\kappa} + O(\gamma^5), \tag{49}$$

which tends to (48) for small γ if $\kappa \simeq 1$. As a whole, the relationships (47) are verified by the present solution exactly, apart from the last expression.

3.4. Closed End Channels

[37] A well-known case is that of a channel forced by the tide seaward and closed landward. Assuming $h^* = 1$, $\theta_h = 0$ in $x_h^* = 0$, and $q^* = 0$ in $x_q^* = L_e^*$, with $L_e^* = L_e/L_s$ the dimensionless length, the boundary conditions (24) and (27) yield

$$a_1^* = \left[1 + \exp(2\Delta L^*)\frac{(\Delta+\gamma/2)}{(\Delta-\gamma/2)}\right]^{-1},$$
$$a_2^* = 1 - a_1^*. \tag{50}$$

The integration constants for velocity, v_1^* and v_2^*, are determined through (20) at the seaward end, and read

$$v_1^* = \frac{-\mathrm{i}a_1^*}{(\Delta-\gamma/2)}, \quad v_2^* = \frac{\mathrm{i}(1-a_1^*)}{(\Delta+\gamma/2)}. \tag{51}$$

It is easy to show that $a_1^* = 0$ and $a_2^* = 1$ for $L^* \to \infty$ (reminding that $\Re(\Delta) = K \geq 0$), thus recovering the solution of section 3.2.

[38] Finding simple explicit relationships for the dependent parameters μ, δ, λ and ϕ from (50)–(51) is a complex task. Nevertheless, we can derive that

$$V^*|_{x^*=0} = v_1^* + v_2^* = \frac{-\gamma/2 + \Delta(1-2a_1^*)}{\widehat{\chi}+\mathrm{i}}, \tag{52}$$

$$\delta_A + \mathrm{i}\lambda_A = \frac{1}{A^*}\frac{dA^*}{dx^*}\bigg|_{x^*=0} = \frac{\gamma}{2} - \Delta(1-2a_1^*), \tag{53}$$

$$\delta_V + \mathrm{i}\lambda_V = \frac{1}{V^*}\frac{dV^*}{dx^*}\bigg|_{x^*=0} = \gamma + \frac{1-\mathrm{i}\widehat{\chi}}{-\gamma/2 + \Delta(1-2a_1^*)}. \tag{54}$$

Although it is not evident, $\delta_V + \mathrm{i}\lambda_V = \delta_A + \mathrm{i}\lambda_A$ for $a_1^* = 0$, as in the case of an infinite estuary (section 3.2). Finally, $\mu = |V^*|$ and the phase lag can be obtained as in (29).

[39] An example of the variation of the main parameters at the mouth with the dimensionless length of the estuary L_e^* is given in Figure 8, where ideal conditions (i.e., no damping) are chosen for the infinite length case, according to (46), and the bed is kept horizontal. Both the linR and linN models reproduce almost perfectly the numerical results, for which no visible effect of ϵ can be noted. It is interesting to note that, for this set of parameters, the effect of the finite length of the channel can be neglected for $L_e^* > 2$. It is also worth noting that, for the same reason, the *Savenije et al.* [2008]

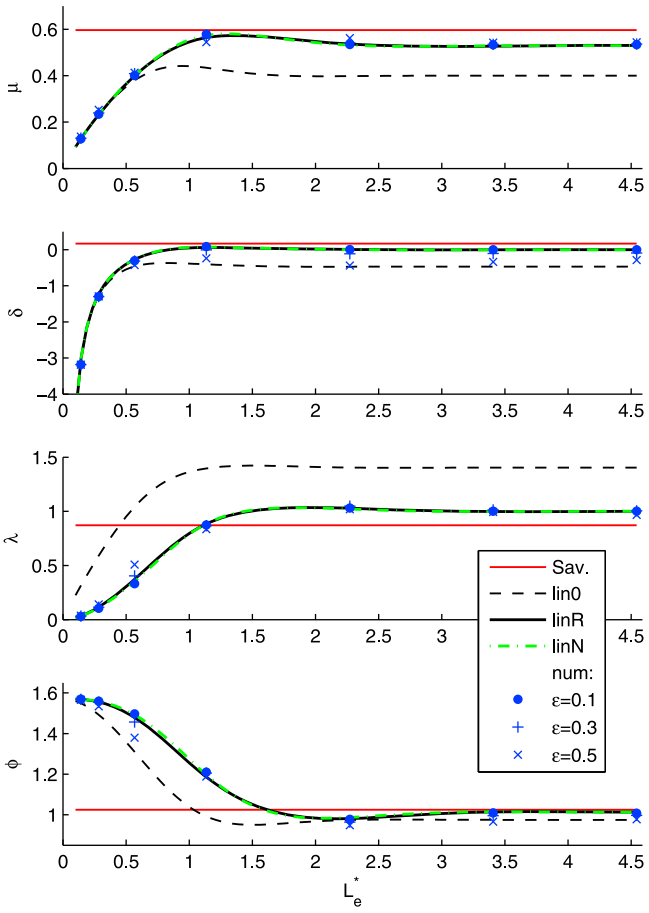

Figure 8. Finite length estuary: main dimensionless parameters (velocity μ, damping δ, wavenumber λ, phase lag ϕ) as a function of the dimensionless length L_e^*. The parameters $\chi = 3.56$ and $\gamma = 1.60$ ($\gamma_Z = 0$) are chosen to have no damping for the infinite length channel. The solution of *Savenije et al.* [2008] for infinite channel is also shown for comparison.

solution is a reasonable approximation when $L_e^* > 1$–1.5 (for this case).

[40] It is important to note that damping and wavenumber are in general not the same for water level and velocity waves. The differences between δ_A and δ_V, and between λ_A and λ_V, are shown in Figure 9. When the channel become shorter, the closed end condition (no flux) causes the velocity damping δ_V to reach large negative values (actually, the decrease of the velocity with x becomes linear along the channel).

3.5. Along-Channel Variation of Parameters and Wave Reflection

[41] The results discussed in sections 3.2 and 3.4 show that the refined linear model with a single reach (linR) predicts the hydrodynamic behavior at the estuary mouth satisfactorily for the velocity scale μ and the wavenumber λ, whereas the total damping δ is significantly dependent on ϵ, and the phase lag ϕ is not so perfectly reproduced even in the limit of small ϵ. On the contrary, the results for ϕ are much better when using multiple reaches (linN). There are two main differences between the linR (single reach) and linN (multiple reaches) models: (1) the linN considers the possible variation of the parameter χ and γ along the estuary and (2) the linN includes the possible effect of wave reflection along the estuary [see also *Jay and Flimchem*, 1997]. In the case of an infinite estuary, the second aspect might seem less relevant, since no wave reflection is expected.

[42] In order to illustrate the behavior of the two models we refer to the case studied in Figure 2, where a convergent, finite length channel ($L_e = 90$ km, $L_b = 60$ km, $L_z = \infty$) is considered. Figure 10 shows the total solution ($|A^*|$, $|V^*|$, black lines), together with the direct wave (i.e., that travelling landward: $|a_2^* \exp(w_2^* x^*)|$, $|v_2^* \exp(w_2^* x^*)|$, blue lines), and the reflected wave ($|a_1^* \exp(w_1^* x^*)|$, $|v_1^* \exp(w_1^* x^*)|$, red lines). The linR model (continuous lines) is compared with the linN model (dashed lines with pluses, corresponding to horizontal bed, $\gamma_Z = 0$), and with a further case having the same value of γ, but generated only by bed exponential variation (dashed lines with crosses, for constant width, $\gamma_B = 0$). When $\gamma_Z = 0$, the main differences regard the velocity: the linR model underestimates both direct and reflected waves in the landward part with respect to linN, although the total solution is very similar. Stronger deviations appear when

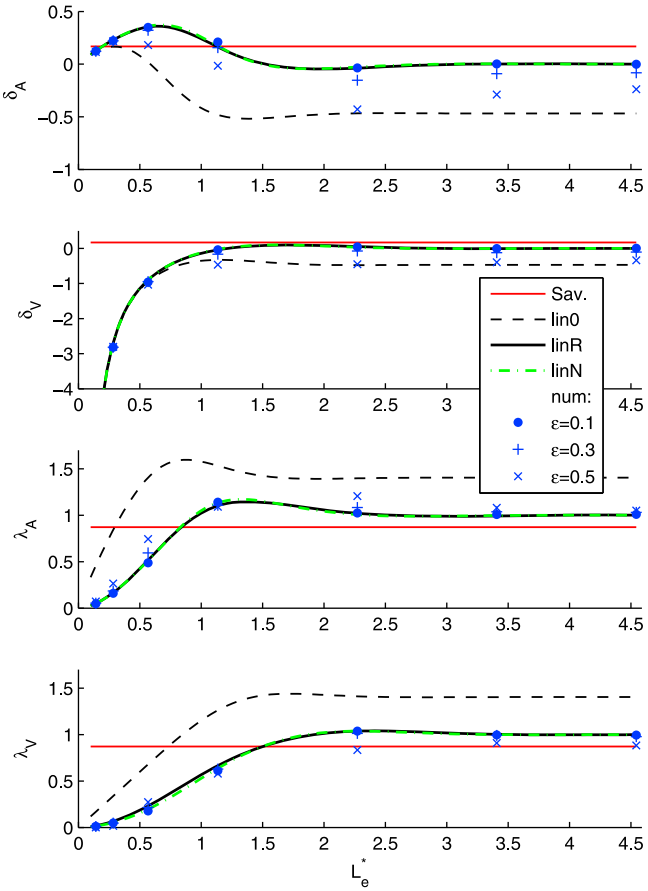

Figure 9. Finite length estuary: dimensionless damping δ_A (water level) and δ_V (velocity) and dimensionless wavenumber λ_A (water level) and λ_V (velocity) as a function of the dimensionless length L_e^*, for the same condition as in Figure 8.

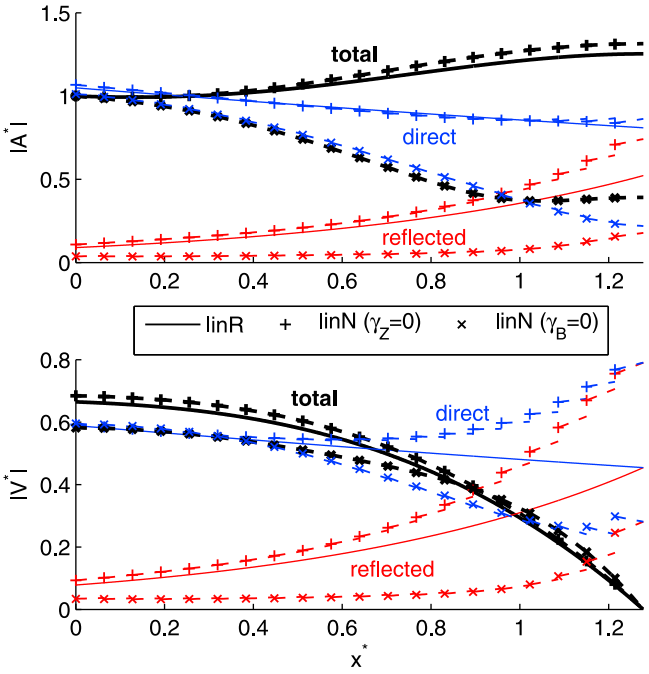

Figure 10. Wave reflection in a closed estuary (γ = 1.17, χ = 3.17): dimensionless amplitudes $|A^*|$ and $|V^*|$. Different colors indicate the total solution (black), the direct wave (blue), and the reflected wave (red). The comparison is made for the same value of γ using linR model (solid lines), width-convergent linN model (dashed lines with pluses, horizontal bed, γ_Z = 0), and depth-convergent linN model (dashed lines with crosses, constant width, γ_B = 0).

considering only depth convergence (γ_B = 0): in this case, according to the linN model (the linR solution does not change, since the value of γ is the same), the reflected wave is less intense, the total solution for $|A^*|$ is damped and the velocity is lower.

[43] It is reasonable that wave reflection is primarily caused by the closed channel end. Therefore, it is worth having a look at the corresponding infinite channel case (i.e., with exactly the same parameters but with a different boundary condition). This is shown in Figure 11: the reflected wave is almost absent. Both water level and velocity waves are more damped in the case of depth convergence, but the solution in the seaward part is the same. This suggests that, when the reflected wave is vanishing, the solution at the mouth is locally controlled by the outer forcing (sea tide), and the effect of depth variation is not different from that of width variation. Moreover, the reflected wave is negligible when γ_Z = 0 (on the contrary being small but visible in the case of depth reduction), implying that width convergence does not cause any reflection [see also *Friedrichs and Aubrey*, 1994]. The partial reflection in the case with γ_Z > 0 is likely due to the reduction of the wave celerity with decreasing depth implicit in (4).

4. Conclusions

[44] We have shown that a suitably formulated version of the linear model for tidal wave propagation is able to correctly reproduce the dynamics of the main harmonic constituent of water level and velocity oscillations for not too large values of the dimensionless tidal amplitude (approximately ϵ < 0.5). Three major points have been recognized by comparing the linear model results with numerical simulations: (1) the effect of width and depth convergence, together with the possibly finite length of the channel, must be taken into account, at least in an approximate way; (2) the friction constant r in Lorentz's linearization of the bed shear stress (equation 5) can, and has to, be calculated within the model and iteratively corrected; and (3) the description of wave propagation can be improved by dividing the estuary in reaches and solving the linear system of the along-channel variable coefficient of the linear wave (linN model).

[45] The iteratively refined model provides good approximations of the main features of the tidal wave at the estuary mouth also when the single-reach version (linR model) is used, in particular in the case of infinitely long channels or for short closed channels. It is worth noting that the dimensionless velocity at the mouth μ is almost independent of the dimensionless amplitude ϵ (at least explicitly, since an indirect effect is included in χ [see also *Toffolon et al.*, 2006]), whereas the most sensitive quantity is the damping parameter δ, followed by the phase lag ϕ between velocity and water level.

[46] We have also compared the performance of the present solutions with the *Savenije et al.* [2008] model, which however is strictly valid only for infinite estuaries: results coincide exactly in the frictionless limit, and are similar far from the threshold between sub- and supercritical conditions. Since the discontinuous behavior predicted by *Savenije et al.* [2008] does not seem to have a counterpart in numerical results (unless in almost frictionless conditions), such a threshold should be considered only as an approxi-

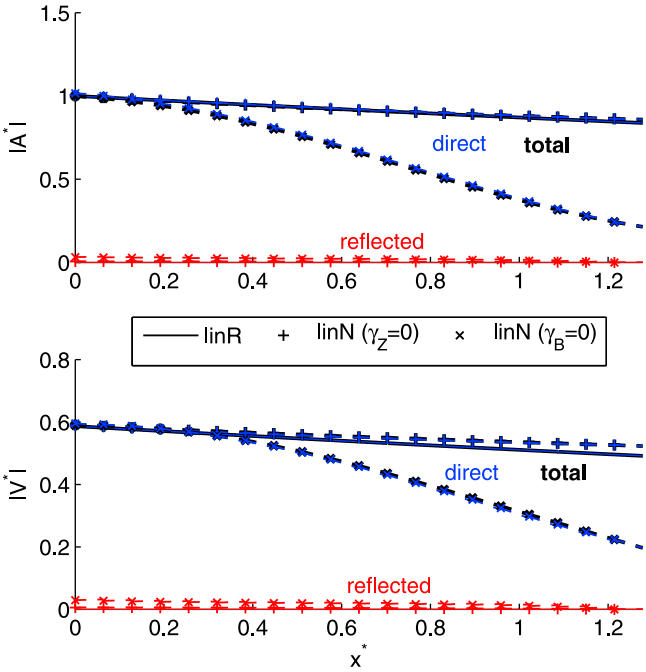

Figure 11. Wave reflection in an open estuary (infinite length, γ = 1.17, χ = 3.17). See the caption of Figure 10.

mate distinction between two qualitatively hydrodynamic configurations.

[47] Finally, we note that focusing on simplified hydrodynamics in estuary is not a trivial matter, in particular in those practical cases where few measurements are available. For instance, the method allows one to estimate a reliable value of the velocity in a simple way by knowing few geometrical data and the tidal forcing at the mouth. This can be particularly crucial when studying salt intrusion [*Savenije*, 2005]. Moreover, the possibility to easily apply the linear model to multiple branching estuaries may give valuable information about the behavior of complex systems.

Appendix A: Characteristic Parameters From Complex Solution

[48] In this section we show how to derive the main characteristic parameters starting from the solution in complex form. Let us consider the water level wave described by $A\cos(\omega t + \phi_A)$, as in (9). The amplitude and phase are given by

$$A(x) = \epsilon D_s \sqrt{\Re\left(A^*\right)^2 + \Im\left(A^*\right)^2}, \tag{A1}$$

$$\phi_A(x) = kx = \arctan\left[\frac{\Im\left(A^*\right)}{\Re\left(A^*\right)}\right], \tag{A2}$$

where $k = 2\pi/L_A$ is the actual dimensional wavenumber (possibly varying along x). Then, following the definitions of Table 2, the dimensionless damping coefficient is given by

$$\delta_A = \frac{1}{A}\frac{\mathrm{d}A}{\mathrm{d}x^*} = \frac{1}{|A^*|^2}\left[\Re(A^*)\frac{\mathrm{d}\Re(A^*)}{\mathrm{d}x^*} + \Im(A^*)\frac{\mathrm{d}\Im(A^*)}{\mathrm{d}x^*}\right], \tag{A3}$$

and the dimensionless wavenumber can be obtained as

$$\lambda_A = \frac{\mathrm{d}\phi_A}{\mathrm{d}x^*} = \frac{1}{|A^*|^2}\left[\Re(A^*)\frac{\mathrm{d}\Im(A^*)}{\mathrm{d}x^*} - \Im(A^*)\frac{\mathrm{d}\Re(A^*)}{\mathrm{d}x^*}\right] \tag{A4}$$

The sum $\delta_A + \mathrm{i}\lambda_A$ obtained by the right hand sides of (A3) and (A4) can also be cast in the form

$$\frac{1}{A^*}\frac{\mathrm{d}A^*}{\mathrm{d}x^*} = \frac{1}{|A^*|^2}\left\{\left[\Re(A^*)\frac{\mathrm{d}\Re(A^*)}{\mathrm{d}x^*} + \Im(A^*)\frac{\mathrm{d}\Im(A^*)}{\mathrm{d}x^*}\right] + \mathrm{i}\left[\Re(A^*)\frac{\mathrm{d}\Im(A^*)}{\mathrm{d}x^*} - \Im(A^*)\frac{\mathrm{d}\Re(A^*)}{\mathrm{d}x^*}\right]\right\}, \tag{A5}$$

from which it is straightforward to obtain (30)–(31). Analogous considerations hold for the velocity wave.

Appendix B: Solution of Linear System

[49] The internal conditions (32)–(33) can be cast in the form of a linear system and solved to give

$$\begin{aligned} a^*_{1,j} &= F_{1,j}a^*_{1,j+1} + G_{1,j}a^*_{2,j+1}, \\ a^*_{2,j} &= F_{2,j}a^*_{1,j+1} + G_{2,j}a^*_{2,j+1}, \end{aligned} \tag{B1}$$

where

$$\begin{aligned} F_{1,j} &= \frac{\sqrt{\alpha_j}w^*_{2,j}\left(w^*_{1,j} - \sqrt{\alpha_j}w^*_{2,j+1}\right)}{\left(w^*_{1,j} - w^*_{2,j}\right)w^*_{2,j+1}\exp\left(w^*_{1,j}L^*_j\right)}, \\ G_{1,j} &= \frac{\sqrt{\alpha_j}w^*_{2,j}\left(w^*_{1,j} - \sqrt{\alpha_j}w^*_{1,j+1}\right)}{\left(w^*_{1,j} - w^*_{2,j}\right)w^*_{1,j+1}\exp\left(w^*_{1,j}L^*_j\right)}, \\ F_{2,j} &= -\frac{\sqrt{\alpha_j}w^*_{1,j}\left(w^*_{2,j} - \sqrt{\alpha_j}w^*_{2,j+1}\right)}{\left(w^*_{1,j} - w^*_{2,j}\right)w^*_{2,j+1}\exp\left(w^*_{2,j}L^*_j\right)}, \\ G_{2,j} &= -\frac{\sqrt{\alpha_j}w^*_{1,j}\left(w^*_{2,j} - \sqrt{\alpha_j}w^*_{1,j+1}\right)}{\left(w^*_{1,j} - w^*_{2,j}\right)w^*_{1,j+1}\exp\left(w^*_{2,j}L^*_j\right)}. \end{aligned} \tag{B2}$$

[50] In general, the interactions between the reaches j and $j + n$ are described by

$$\begin{aligned} a^*_{1,j} &= F^{(n)}_{1,j}a^*_{1,j+n} + G^{(n)}_{1,j}a^*_{2,j+n}, \\ a^*_{2,j} &= F^{(n)}_{2,j}a^*_{1,j+n} + G^{(n)}_{2,j}a^*_{2,j+n}, \end{aligned} \tag{B3}$$

where the rules

$$\begin{aligned} F^{(n)}_{1,j} &= F^{(n-1)}_{1,j+1}F_{1,j} + F^{(n-1)}_{2,j+1}G_{1,j}, \\ G^{(n)}_{1,j} &= G^{(n-1)}_{1,j+1}F_{1,j} + G^{(n-1)}_{2,j+1}G_{1,j}, \\ F^{(n)}_{2,j} &= F^{(n-1)}_{1,j+1}F_{2,j} + F^{(n-1)}_{2,j+1}G_{2,j}, \\ G^{(n)}_{2,j} &= G^{(n-1)}_{1,j+1}F_{2,j} + G^{(n-1)}_{2,j+1}G_{2,j} \end{aligned} \tag{B4}$$

represent an iterative backward construction of the coefficients ($n \geq 2$), starting from $F^{(1)}_{m,j} = F_{m,j}$, $G^{(1)}_{m,j} = G_{m,j}$ ($m = 1, 2$, $j = N - 1$).

[51] Therefore, the linear system can be translated into a couple of equations linking the seaward reach ($j = 1$) to the landward one ($j = N$). The seaward boundary condition $a^*_{1,1} + a^*_{2,1} = 1$ yields

$$\left[F^{(N-1)}_{1,1} + F^{(N-1)}_{2,1}\right]a_{1,N}{}^* + \left[G^{(N-1)}_{1,1} + G^{(N-1)}_{2,1}\right]a^*_{2,N} = 1. \tag{B5}$$

Therefore, imposing a landward boundary condition in the form $a^*_{1,N} = \psi a^*_{2,N}$, where

$$\psi = -\frac{w^*_{2,N}}{w^*_{1,N}}\exp\left[\left(w^*_{2,N} - w^*_{1,N}\right)L^*_j\right] \tag{B6}$$

for the closed boundary and $\psi = 0$ for the infinite channel, the condition (B5) gives

$$a^*_{2,N} = \left\{\left[F^{(N-1)}_{1,1} + F^{(N-1)}_{2,1}\right]\psi + \left[G^{(N-1)}_{1,1} + G^{(N-1)}_{2,1}\right]\right\}^{-1}. \tag{B7}$$

Once that $a^*_{1,N}$, $a^*_{2,N}$ are determined, the other unknowns can be reconstructed using (B1) backward.

[52] We note that this method, although theoretically usable to determine the solution of the linear system

explicitly, is affected by accumulation of numerical errors and may give unreliable results also for relatively small values of N.

Notation

Main variables (asterisk denotes dimensionless variable)

- x,x^* longitudinal coordinate.
- t,t^* temporal coordinate.
- D instantaneous depth.
- Y,Y^* tidally averaged depth.
- H free surface elevation.
- Z,Z^* bed elevation.
- B width.
- U velocity.
- $\widehat{U}$ reference velocity for Lorentz's linearation.
- A, $|A^*|$ amplitude of free surface oscillation (first mode), with A^* a complex number.
- V, $|V^*|$ amplitude of velocity oscillation (first mode), with V^* a complex number.
- τ bed shear stress.
- C_h dimensionless Chézy parameter.
- σ storage ratio.
- T, ω tidal period, frequency.
- ρ water density.
- g gravity acceleration.
- L_e, L_e^* channel length.
- r Lorentz's linearized friction factor.
- κ Lorentz's linearization constant.

Variables defined for the estuary reach (subscript s denotes the reference values defined at the seaward end)

- A_s tidal wave amplitude.
- V_s velocity amplitude.
- C_s frictionless wave celeriy.
- D_s (= Y_s) reference depth.
- B_s reference width.
- L_s intrinsic length scale.
- L_b, L_z exponential convergence length (width, depth).
- L_A, L_V wave lengths (free surface, velocity).
- C_A, C_V wave celerity (free surface, velocity).

Dimensionless parameters (see also Tables 1 and 2)

- ϵ tidal amplitude.
- γ total convergence.
- γ_B, γ_Z width, depth convergence.
- χ friction.
- $\widehat{\chi}$ linearized friction parameter.
- μ velocity scale.
- δ damping.
- δ_A, δ_V free surface, velocity damping.
- ϕ phase lag.
- ϕ_A, ϕ_V phase (free surface, velocity).
- λ wavenumber.
- λ_A, λ_V wavenumber (free surface, velocity).

Dimensionless variables used in the complex solution

- Γ distance from critical convergence.
- Δ complex parameter.
- K, Ω real parameters.
- a_1^*, a_2^* complex coefficients (for wave amplitude).
- v_1^*, v_2^* complex coefficients (for velocity).
- w_1^*, w_2^* complex coefficients ($w_l^* = m_l^* + ik_l^*$).
- m_1^*, m_2^* amplification factors.
- k_1^*, k_2^* wavenumbers.

[53] **Acknowledgments.** The work of the first author has been partially cofunded by the Italian Ministry of Education, University and Research (MIUR) within the project "Eco-morfodinamica di ambienti a marea e cambiamenti climatici" (PRIN 2008).

References

Dronkers, J. J. (1964), *Tidal Computations in River and Coastal Waters*, 518 pp., Elsevier, New York.

Friedrichs, C., and D. Aubrey (1994), Tidal propagation in strongly convergent channels, *J. Geophys. Res.*, *99*, 3321–3336, doi:10.1029/93JC03219.

Giese, B. S., and D. A. Jay (1989), Modelling tidal energetics of the Columbia River Estuary, *Estuarine Coastal Shelf Sci.*, *29*, 549–571, doi:10.1016/0272-7714(89)90010-3.

Jay, D. A. (1991), Green's law revisited: Tidal long-wave propagation in channels with strong topography, *J. Geophys. Res.*, *96*, 20,585–20,598, doi:10.1029/91JC01633.

Jay, D. A., and E. P. Flimchem (1997), Interaction of fluctuating river flow with a barotropic tide: A demonstration of wavelet tidal analysis methods, *J. Geophys. Res.*, *102*, 5705–5720, doi:10.1029/96JC00496.

Kukulka, T., and D. A. Jay (2003), Impacts of Columbia River discharge on salmonid habitat: 1. A nonstationary fluvial tide model, *J. Geophys. Res.*, *108*(C9), 3293, doi:10.1029/2002JC001382.

Lanzoni, S., and G. Seminara (1998), On tide propagation in convergent estuaries, *J. Geophys. Res.*, *103*, 30,793–30,812, doi:10.1029/1998JC900015.

Lorentz, H. A. (1926), *Verslag Staatscommissie Zuiderzee*, Alg. Landsdrukkerij, The Hague, Netherlands.

Savenije, H. H. G. (2005), *Salinity and Tides in Alluvial Estuaries*, Elsevier, New York.

Savenije, H. H. G., M. Toffolon, J. Haas, and E. J. M. Veling (2008), Analytical description of tidal dynamics in convergent estuaries, *J. Geophys. Res.*, *113*, C10025, doi:10.1029/2007JC004408.

Seminara, G., S. Lanzoni, N. Tambroni, and M. Toffolon (2010), How long are tidal channels?, *J. Fluid Mech.*, *643*, 479–494, doi:10.1017/S0022112009992308.

Souza, A. J., and A. E. Hill (2006), Tidal dynamics in channels: Single channels, *J. Geophys. Res.*, *111*, C09037, doi:10.1029/2006JC003469.

Speer, P. E., and D. G. Aubrey (1985), A study of non-linear tidal propagation in shallow inlet/estuarine systems, *Estuarine Coastal Shelf Sci.*, *21*, 207–224, doi:10.1016/0272-7714(85)90097-6.

Toffolon, M., and S. Lanzoni (2010), Morphological equilibrium of short channels dissecting the tidal flats of coastal lagoons, *J. Geophys. Res.*, *115*, F04036, doi:10.1029/2010JF001673.

Toffolon, M., G. Vignoli, and M. Tubino (2006), Relevant parameters and finite amplitude effects in estuarine hydrodynamics, *J. Geophys. Res.*, *111*, C10014, doi:10.1029/2005JC003104.

H. H. G. Savenije, Department of Water Management, Delft University of Technology, PO Box 5048, NL-2600 GA Delft, Netherlands. (h.h.g.savenije@tudelft.nl)

M. Toffolon, Department of Civil and Environmental Engineering, University of Trento, Via Mesiano, 77, I-38123 Trento, Italy. (marco.toffolon@ing.unitn.it)